

Effect of Post-spray Shot Peening Treatment on the Corrosion Behavior of NiCr-Mo Coating by Plasma Spraying of the Shell–Core–Structured Powders

Jia-Jia Tian¹ · Ying-Kang Wei¹ · Cheng-Xin Li¹ · Guan-Jun Yang¹ · Chang-Jiu Li¹

Submitted: 17 July 2017 / in revised form: 26 October 2017 / Published online: 16 November 2017
© ASM International 2017

Abstract Corrosion of metal plays a detrimental role in service lifetime of parts or systems. Therefore, coating a protective film which is fully dense and defects free on the base metal is an effective approach to protect the base metal from corrosion. In this study, a dense NiCr-20Mo coating with excellent lamellar interface bonding was deposited by plasma spraying of the novel shell–core–structured Mo-clad-NiCr powders, and then post-spray shot peening treatment by cold spraying of steel shots was applied to the plasma-sprayed NiCr-20Mo coating to obtain a fully dense coating through eliminating possibly existed pores and un-bonded interfaces within the NiCr-20Mo coating. Corrosion behaviors of the NiCr-20Mo coatings before and after shot peening were tested to investigate the effect of the post-spray shot peening on the corrosion behavior of the NiCr-20Mo coating. Results showed that a much dense and uniform plasma-sprayed NiCr-20Mo coating with perfect lamellar bonding at most of interfaces was deposited. However, the electrochemical tests revealed the existence of through-thickness pores in the as-plasma-sprayed NiCr-20Mo coating. Through the post-spray shot peening treatment, a completely dense top layer in the coating was formed, and with the increase in

the shot peening intensity from one pass to three passes, the dense top layer became thicker from 100 μm to reach 300 μm of the whole coating thickness. Thus, a fully dense bulk-like coating was obtained. Corrosion test results showed that the dense coating layer resulting from densification of shot peening can act as an effective barrier coating to prevent the penetration of the corrosive medium and consequently protect the substrate from corrosion effectively. Therefore, a fully dense bulk-like NiCr-20Mo coating with excellent corrosion resistance can be achieved through the plasma spraying of Mo-clad-NiCr powders followed by appropriate post-spray shot peening treatment.

Keywords corrosion · interface bonding · NiCr coating · plasma spraying · post-spray shot peening · shell–core–structured powder

Introduction

Corrosion of metal plays a detrimental role in the lifetime of the engineering part or a system (Ref 1–3). Therefore, a lot of efforts have been made to improve the corrosion resistance of metal parts. It is a consensus that coating a protective film on the base metal is one of the most effective methods to protect the metal from corrosion (Ref 2, 3). That is, coatings can protect the substrate from corrosion by acting as an insulating barrier layer of low solubility between the metal surface and corrosive environment. Nowadays, there are a series of surface technologies available to coat a film on metal substrate, such as electrochemical plating (Ref 4), conversion coatings (Ref 5–8), gas-phase deposition (Ref 9–11), thermal spraying (Ref 12–14), organic coatings (Ref 3, 15) and so on. For example, as one of the most cost effective and

This article is an invited paper selected from presentations at the 2017 International Thermal Spray Conference, held June 7–9, 2017, in Düsseldorf, Germany, that has been expanded from the original presentation.

✉ Chang-Jiu Li
licj@mail.xjtu.edu.cn

¹ State Key Laboratory for Mechanical Behavior of Materials, School of Materials Science and Engineering, Xi'an Jiaotong University, Xi'an 710049, Shaanxi Province, People's Republic of China

simple techniques for introducing a metallic coating to a substrate, electrochemical plating is one of the most commonly used surface technologies (Ref 2, 16, 17). Moreover, the plating can be usually divided into two types: electroplating and electroless plating. In the case of the electroless plating, although it has various advantages, such as great potential to produce uniform, corrosion- and wear-resistant coatings with good electrical conductivity and solderability, at a relative low cost, electroless plating does have some challenges and drawbacks. For instance, there are some serious concerns over waste disposal. That is, the use of toxic chemicals such as chromium compounds, cyanide compounds and fluoride compounds in the pretreatment and plating baths has very detrimental influences on environment and it needs further research into the development of green plating technologies. Moreover, in the term of the electroplating, although it does not have as much environmental impact due to long bath life of the plating solutions, it is difficult to achieve uniform coatings on complex shapes due to its uneven throwing power of the current required for metal deposition (Ref 18, 19).

Accordingly, as a potential alternative technology of electrochemical technologies, thermal spraying is nowadays widely used for the substitution of deposition of hard chrome coating and various kinds of metallic and ceramic coatings due to their environmental friendly features and plentiful kinds of materials can be deposited. For instance, plasma-sprayed nickel or iron-based alloy coatings are widely used to protect the turbine and boiler tube components from corrosion or high-temperature oxidation (Ref 20). However, since plasma-sprayed coatings are formed by successive impact of molten droplets, the coatings always present a typical lamellar microstructure with only a limited interface bonding ratio with a number of un-bonded interfaces and pores. Moreover, it has been proved that the maximum bonding ratio within the plasma spray metallic coating is $\sim 1/3$ with the variation of spray parameters (Ref 21–24), which significantly limits the overall properties of coatings, (Ref 25–27), especially for the anti-corrosion performance. That is, the through-thickness pores, which are formed by the connection of the un-bonded interfaces and pores within a coating, especially for the cathodic metal coating, will provide paths for the corrosive mediums reaching to substrate and consequently lead to the corrosion of substrate. Therefore, fully dense microstructure with well-bonded interfaces and no defects is always required for a cathodic coating to provide corrosion protection for the base metal (Ref 5, 9–11, 15, 22, 28, 29), and any defects within the cathodic coating will significantly affect its corrosion resistance and consequently lead to the failure of corrosion protection. Therefore, how to improve the interface bonding within coating is an important issue waiting to be settled.

Many efforts have been made to improve the interface bonding within plasma-sprayed metallic coatings, such as controlling spraying parameters, increasing the deposition temperature or employing low-pressure plasma spraying. However, it has been proved that these approaches are always not suitable or effective for improving the interface bonding of plasma-sprayed metallic and alloy coatings (Ref 24, 30–32). For instance, in the case of the deposition temperature, when the deposition temperature is increased, oxide film will be readily formed on the surface of substrate or pre-deposited splats, which will significantly hinder the effective metallurgical bonding formation between lamellae.

Therefore, in our previous study, a novel shell–core–structured powder particle, which was designed by cladding spherical NiCr particle with refractory Mo, was proposed to restrict the evaporation of low melting point elements and increase the particle temperature high enough during in-flight to induce localized substrate melting and metallurgical interface bonding (Ref 33). Results showed that a dense NiCr-20Mo coating with much improved interface bonding was obtained. Moreover, localized substrate melting and strong metallurgical bonding were found to be formed at splat–substrate interface attributing to the much enhanced particle temperature, which was confirmed numerically and experimentally. However, due to the separation of the shell Mo from the NiCr core during in-flight process of the mechanical-alloyed NiCr-20Mo particle, there existed some Mo inclusions within the NiCr-20Mo coating, which would hinder the effective bonding between lamellae. Thus, in this study, the optimized NiCr-20Mo coating was prepared by plasma spraying of the heat-treated mechanical-alloyed NiCr-20Mo powder particles to obtain an uniform and much denser coating with further improved interface bonding. Furthermore, post-spray shot peening treatment by cold spraying of spherical steel shots was applied to the as-plasma-sprayed NiCr-20Mo coating to achieve a fully dense coating. Moreover, the effects of shot peening on the microstructure and the corrosion behavior of the NiCr-20Mo coatings were investigated.

Experimental Procedures

Powder Preparation

The mechanical-alloyed Mo-clad NiCr powders, which were referred to as the NiCr-20Mo powders, were prepared by ball milling process with sub-micrometer Mo and spherical NiCr powder with a size range from 50 to 75 μm , and the detailed process parameters were set to be the same as that in our previous study (Ref 33). The NiCr-20Mo powders with a 20 vol.% of Mo were referred to as NiCr-20Mo powders. In order to suppress the separation of shell

Mo from the core NiCr, heat treatment was employed for the mechanical-alloyed NiCr-20Mo powders at a sintering condition of 1000 °C for 30 min. Figure 1 shows the cross-sectional microstructures and surface morphology of the heat-treated mechanical-alloyed NiCr-20Mo powder. It can be seen that a dense Mo shell layer was clad around the spherical NiCr core with an interlayer, which provides metallurgical bonding between Mo shell and NiCr core.

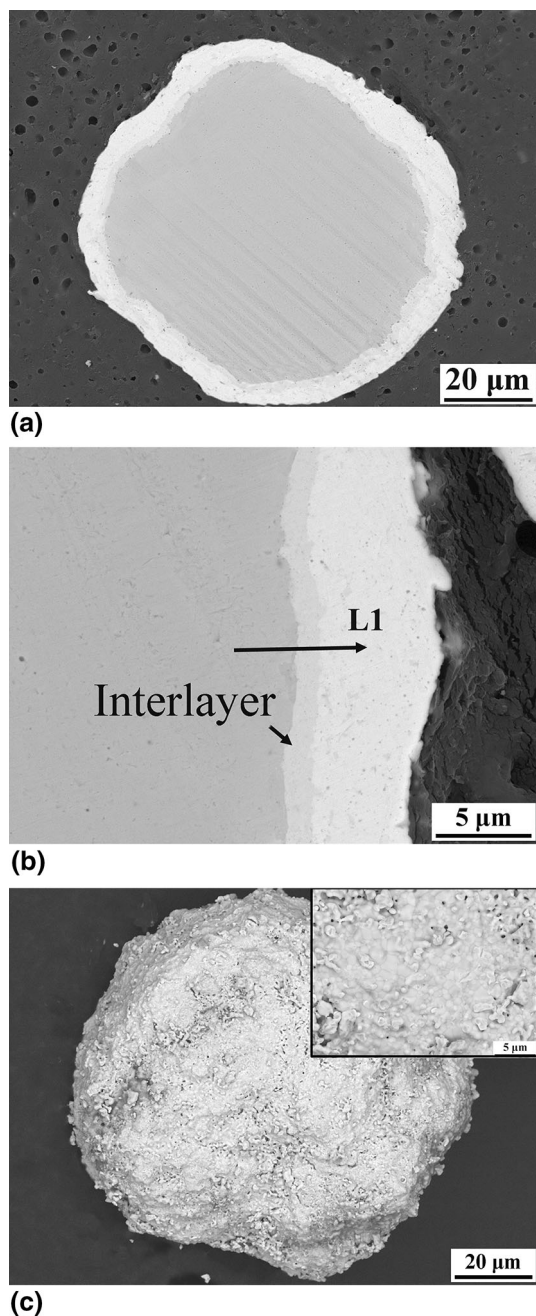


Fig. 1 a, b Cross-sectional microstructures, and c surface morphology of typical NiCr-20Mo powder

Preparation of Plasma-Sprayed NiCr-20Mo Coating

The NiCr-20Mo coating was deposited onto a grit-blasted Q235 mild steel substrate by plasma spraying of the heat-treated NiCr-20Mo powders using a commercial plasma spray system (80 kW, Jiujiang, China). An Ar gas shrouded plasma spray torch was used to reduce the particle oxidation during in-flight process. The spray power and spray distance were set as 42 kW and 140 mm, respectively. Moreover, the flow rates of the primary gas (Ar) and the secondary gas (H₂) were set as 45 and 9 L/min, respectively.

Post-spray Shot Peening Treatment for the Plasma-Sprayed NiCr-20Mo Coatings

Shot peening is a widely used surface strengthening method to improve the service performance of structural metallic materials, such as the high cycle fatigue performance (Ref 34, 35). Moreover, shot peening is also employed to increase the coating density and therefore improve the corrosion resistance of a coating (Ref 12, 14). Cold spray has gained considerable interest in recent years as a method to deposit uniform and dense coating due to the very high particle velocity and much lower particle temperature (Ref 36–38). In this study, post-spray shot peening treatment was applied to the as-plasma-sprayed NiCr-20Mo coating to eliminate the possible pores within coating, which was conducted by cold spraying of spherical 1Cr18 stainless steel (S30210, GB/T 20878) particles with a size range from 200 to 300 μm using a cold spray system (DWCS-2000, Shaanxi Dewei Automation Equipment Co, Shaanxi, China). The feed rate of the peening particle was kept at 35 g/min, and the transverse speed of the cold spray nozzle was 80 mm/s. In addition, the distance between the cold spray nozzle exit and the coating was set as 20 mm. The accelerating gas used for accelerating particles was N₂, and the stagnation pressure and temperature of the accelerating gas were set as 1 MPa and 200 °C, respectively. In order to investigate the effect of shot peening intensity on the microstructure and corrosion performances of the NiCr-20Mo coating, different shot peening passes were used as a variable to characterize the shot peening intensity.

Characterization of the Coating

The cross-sectional microstructures of the as-plasma-sprayed and shot-peened NiCr-20Mo coatings were examined using scanning electron microscopy (SEM, MIRA 3 LMH, TESCAN, Czech) equipped with energy-dispersive spectroscopy (EDS).

Tensile Strength Test

Tensile strength tests were performed in accordance with the widely used ASTM C633-79 standard (Ref 39). The detailed methods have been described in Ref 33.

Corrosion Test

Corrosion behaviors of Q235 steel (GB/T709-2006) samples coated by different coatings were evaluated through their polarization behavior by electrochemical method using a CS310 electrochemical workstation (Corrtest Instruments CO., Ltd, Wuhan, China), which were conducted by the commonly used three-electrode method. The parameters used for the electrochemical tests are listed in Table 1. A 3.5% NaCl aqueous solution with a PH of 7 was prepared as the electrolyte. The corrosion test was conducted at a temperature of 25 °C. Moreover, the sample surfaces were all firstly ground by a 1000-grit SiC abrasive paper and then mirror-polished by a 0.1 μm diamond polish agent to control an accurate corrosion area accurately and eliminate the influence of the surface roughness on the corrosion behavior. The corrosion sample was with a dimension of 30 mm × 15 mm × 1.5 mm. The samples were embedded in a resin adhesive for sealing leaving an exposed surface area of 10 mm × 10 mm for corrosion test. Moreover, an area of 10 mm × 15 mm at the end of sample was exposed for electrical connection to the test system through an alligator clip. Prior to the polarization tests, the open circuit potentials (E_{ocp}) of samples were firstly tested at a stable stage with a fluctuation of the E_{ocp} less than 10 mV in 5 min. In addition, the cross-sectional microstructure of the corroded coating after electrochemical test was examined by SEM and the chemical composition of the corrosion products was analyzed by EDS. The coated samples after electrochemical test were firstly sawed and mounted into epoxy resin and then ground by SiC abrasive paper after they were solidified and finally polished by a 0.1 μm diamond polish agent. The samples were then ultrasonically cleaned twice in an ethanol bath for 5 min to remove the adhered polish agent. For comparison, the natural potential and polarization behavior of

the blasted Q235 substrate and the free-standing NiCr-20Mo coating film were also examined. The plasma-sprayed NiCr-20Mo coating was firstly deposited onto an aluminum substrate, and then the aluminum substrate was ground off to obtain the free-standing NiCr-20Mo coating film.

Results

Microstructures of the As-Plasma-Sprayed and Shot-Peened NiCr-20Mo Coatings

Microstructure of the As-Plasma-Sprayed NiCr-20Mo Coating

Figure 2 shows the microstructures of the plasma-sprayed NiCr-20Mo coating. As can be seen in Fig. 2(a), a very dense and uniform coating with no Mo inclusions and almost no obvious pores and un-bonded interfaces was obtained. Moreover, Fig. 2(b) showing a closer view of the NiCr-20Mo coating reveals that a little amount of small pores and un-bonded interfaces were distributed within the

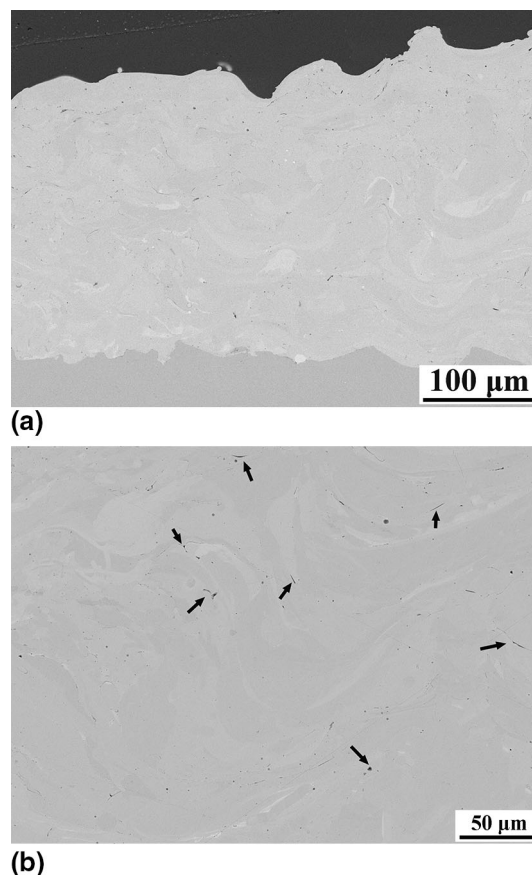


Fig. 2 **a** Cross-sectional microstructure of the as-plasma-sprayed NiCr-20Mo coating; **b** is a closer view

Table 1 Electrochemical test parameters

Parameters	Values
Reference electrode (RE)	Saturated calomel electrode
Counter electrode (CE)	Platinum electrode
Work electrode (WE)	Tested samples
Electrolyte	3.5% NaCl aqueous solution
Scanning method	Potentiodynamic
Scanning speed (mV/s)	0.5

coating. Those small defects possibly resulted from the limited wetting of lower temperature spreading melt front at the very periphery region during splatting. Since most of the central portion of the splat is bonded to the substrate perfectly due to the impact-induced melting of substrate by the ultra-high-temperature NiCr-20Mo particles, only a small portion of the splat at the very periphery region is weakly bonded to the substrate. That is because at the end stage of the spreading, the splat temperature of melt at the periphery region decreases to a lower value which is not high enough to form effective bonding with substrate. Therefore, a dense and uniform coating with perfect bonding at most of interfaces and only a small number of tiny pores and un-bonded interfaces were present in the plasma-sprayed NiCr-20Mo coating.

Microstructure of the Shot-Peened Plasma-Sprayed NiCr-20Mo Coating

Since the recent investigation revealed that in comparison with the brittle feature of conventional plasma-sprayed NiCr coating under particle erosion, the NiCr-20Mo

coating presents the same ductile behavior as that of nickel-based bulk alloy, the post-spray shot peening treatment was conducted for the plasma-sprayed NiCr-20Mo coating to obtain possible further densification and even cold welding effect to eliminate tiny pores within coating. Different shot peening passes for the NiCr-20Mo coating were set as a variable to characterize the effect of shot peening intensity, while other parameters were set as constants. The cross-sectional microstructures of the shot-peened NiCr-20Mo coating with different shot peening passes are shown in Fig. 3, 4 and 5. It was obviously found that after shot peening treatment, the coatings present distinctly two-layer structure. At the top surface of the shot-peened NiCr-20Mo coating, pores and un-bonded interfaces as observed in Fig. 2 disappeared, exhibiting a dense microstructure with small oxide particles in a gray contrast distributed in. This fact means that tiny pores are closed off due to the tamping effect of the shot peening particles. Moreover, it was also found that with the increase in the shot peening intensity, which is the shot peening passes, the dense top layer became thicker from 100 to 200 μm and finally reached to the whole coating thickness of 300 μm . In this way, all the

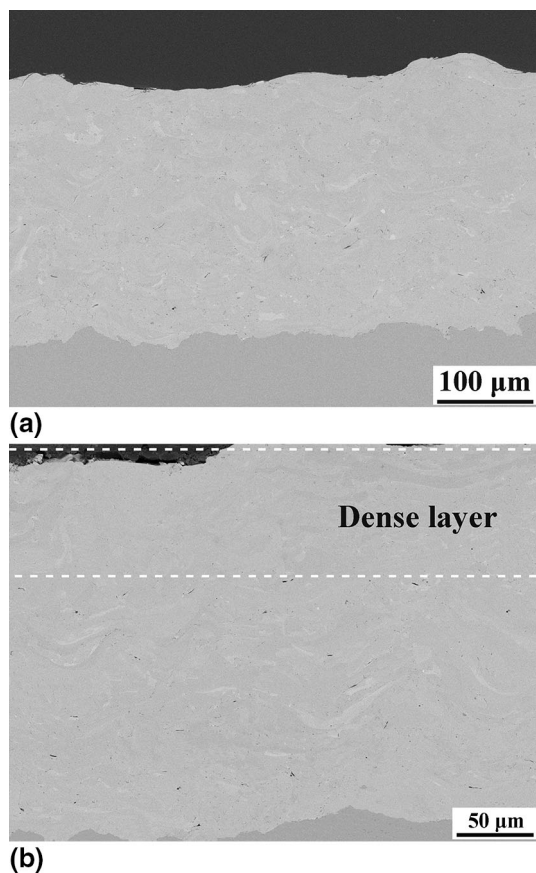


Fig. 3 a Cross-sectional microstructure of the one-pass shot-peened NiCr-20Mo coating; b is a closer view

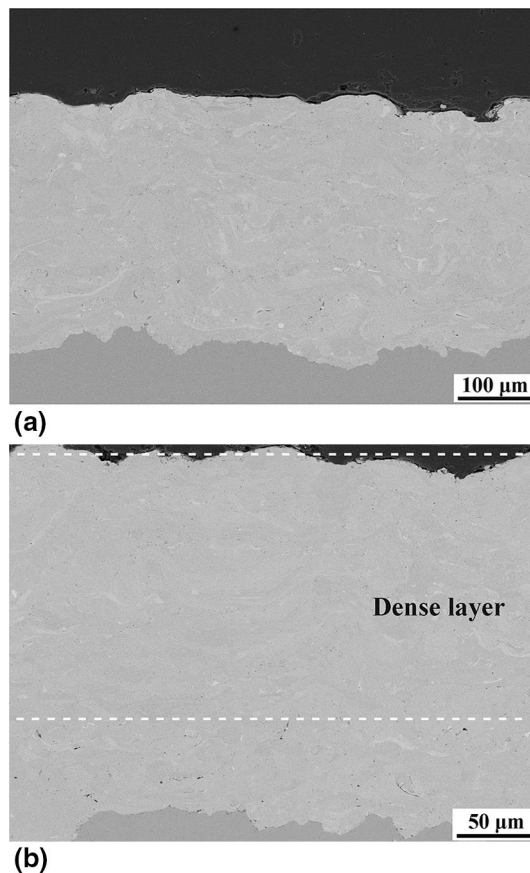
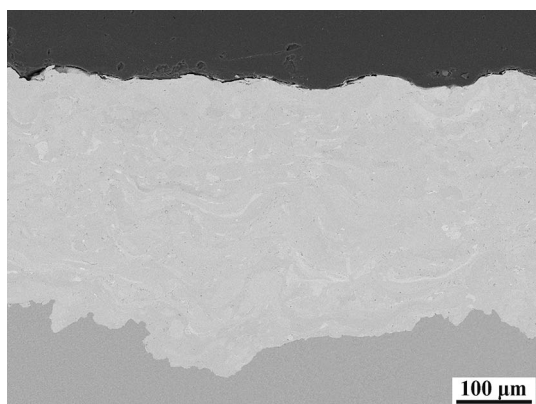
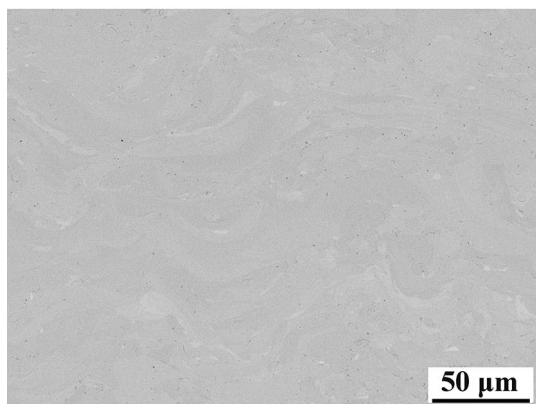


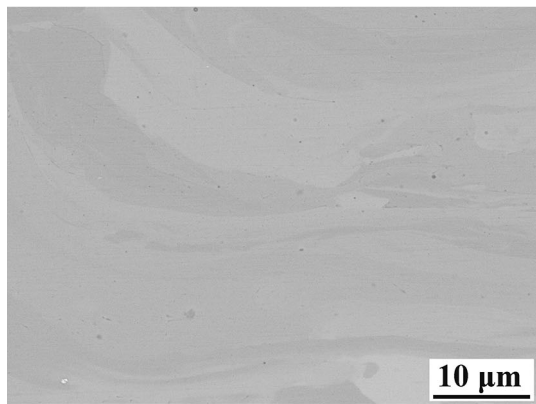
Fig. 4 a Cross-sectional microstructure of the two-pass shot-peened NiCr-20Mo coating; b is a closer view



(a)



(b)



(c)

Fig. 5 a Cross-sectional microstructure of the three-pass shot-peened NiCr-20Mo coating; b, c are the closer views

remaining pores within coating was closed off and consequently a fully dense NiCr-20Mo coating was obtained after the three-pass shot peening. Furthermore, apparent porosities within coatings were measured by the image analysis methods. As shown in Fig. 6, the apparent porosity within coating decreased gradually from 0.16% of the as-plasma-sprayed NiCr-20Mo coating to 0.1, 0.06% and finally to 0.04% of the three-pass shot-peened NiCr-20Mo coating, which can be considered as a fully dense coating. Thus, it can be concluded that the NiCr-20Mo

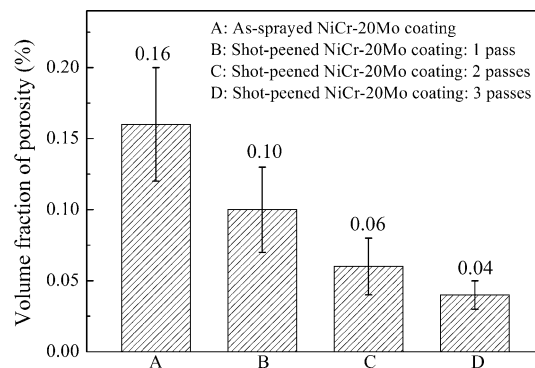


Fig. 6 Apparent porosities of the as-plasma-sprayed NiCr-20Mo coating and the shot-peened NiCr-20Mo coating with different passes

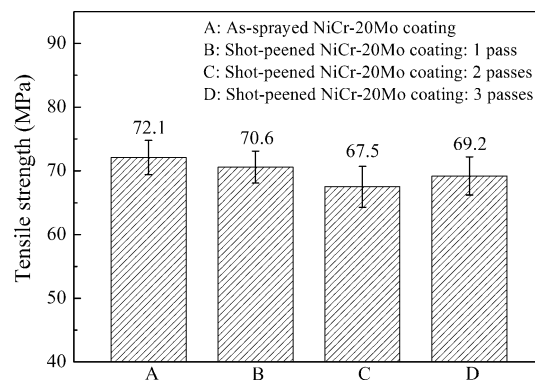
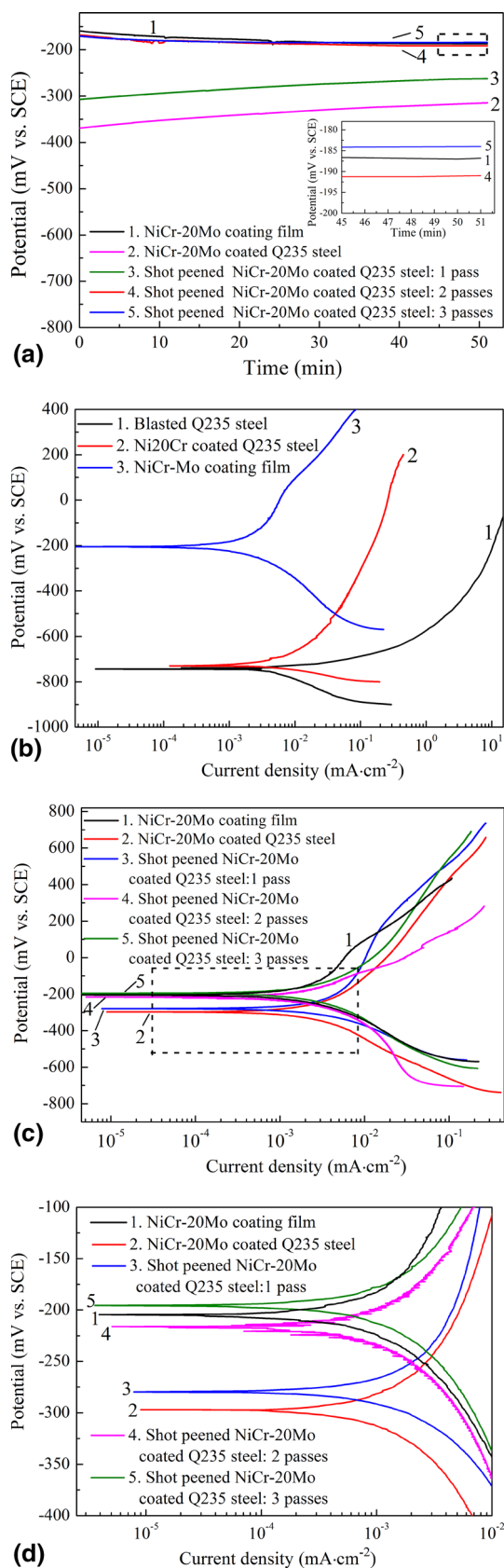


Fig. 7 Tensile strengths of the as-plasma-sprayed NiCr-20Mo coating and the shot-peened NiCr-20Mo coating with different passes

coating became denser with the increase in the shot peening passes and consequently a fully dense bulk-like coating with no defects was obtained for the 300 μm NiCr-20Mo coating when the shot peening passes reached to 3.

Tensile test was performed to measure adhesive strength of the plasma-sprayed NiCr-20Mo coatings with and without post-spray shot peening treatment. Results showed that all the sample couples detached at glue adhesive. That is, both the adhesive strength and the cohesive strength of all the coatings are higher than the obtained glue strength and the real strength of coatings cannot be obtained by this method. It can be seen in Fig. 7 that all the coatings detached from glue with a mean strength of about 70 MPa. In this way, it was revealed that the shot-peened NiCr-20Mo coating still exhibits excellent interface bonding.

In addition, the plasma-sprayed NiCr coating was also subjected to post-spray shot peening treatment for comparison. However, the whole coating spalled off from substrate during one-pass shot peening due to low coating–substrate adhesive strength. Therefore, the shot peening under the present condition in this study is only effective for the ductile coatings that have high adhesive strength.



◀**Fig. 8** **a** Open circuit potential curves; **b** potentiodynamic polarization curves of blasted Q235 steel, NiCr-coated Q235 steel and NiCr-20Mo coating film; **c** potentiodynamic polarization curves of the as-plasma-sprayed NiCr-20Mo-coated Q235 steel and the shot-peened NiCr-20Mo-coated Q235 steel with different passes; **d** high magnification graph of the rectangular region in (c)

Table 2 Potentiodynamic polarization and Tafel extrapolation results

Samples	E_{ocp} , mV	E_{corr} , mV	i_{corr} , mA/cm ²
Blasted Q235 steel	-749	-743	4.16E-3
Ni20Cr-coated Q235 steel	-733	-728	3.91E-3
NiCr-20Mo coating film	-186	-204	4.41E-4
NiCr-20Mo-coated Q235 steel	-315	-297	7.97E-4
Shot-peened NiCr-20Mo-coated Q235 steel: one pass	-263	-286	6.56E-4
Shot-peened NiCr-20Mo-coated Q235 steel: two passes	-191	-210	4.82E-4
Shot-peened NiCr-20Mo-coated Q235 steel: three passes	-184	-196	4.96E-4

Effect of the Post-spray Shot Peening Treatment on the Corrosion Behavior of NiCr-20Mo Coating

In order to investigate the effect of shot peening on the corrosion behaviors of the NiCr-20Mo coatings, the electrochemical behavior of the NiCr-20Mo coatings before and after post-spray shot peening treatment was examined. The open circuit potential (E_{ocp}) and potentiodynamic polarization curves were tested, as shown in Fig. 8, and the corresponding E_{ocp} , E_{corr} and i_{corr} are listed in Table 2, which were obtained from an average value of five tests. For comparison, the polarization behaviors of Q235 steel, NiCr-coated Q235 steel sample and free-standing NiCr-20Mo coating film were also tested and the corresponding curves are shown in Fig. 8(b). It is obvious that NiCr-coated Q235 steel sample presented the same electrochemical behavior as that of the bare steel due to large amount of through-thickness pores in the coating. On the contrast, it was found that the E_{ocp} and E_{corr} of the plasma-sprayed NiCr-20Mo-coated Q235 steel sample presented a significant increment toward noble and the i_{corr} exhibited a dramatic decrease compared with that of NiCr-coated Q235 steel. The obviously improved corrosion resistance of the NiCr-20Mo coating is attributed to the near perfectly bonded lamellar interfaces, resulting from the impact-induced melting of substrate surface by high-temperature NiCr-20Mo molten droplets. However, as can be seen in Fig. 8(a), since the E_{ocp} of NiCr-20Mo-coated Q235 steel sample is 130 mV negative than that of free-standing NiCr-

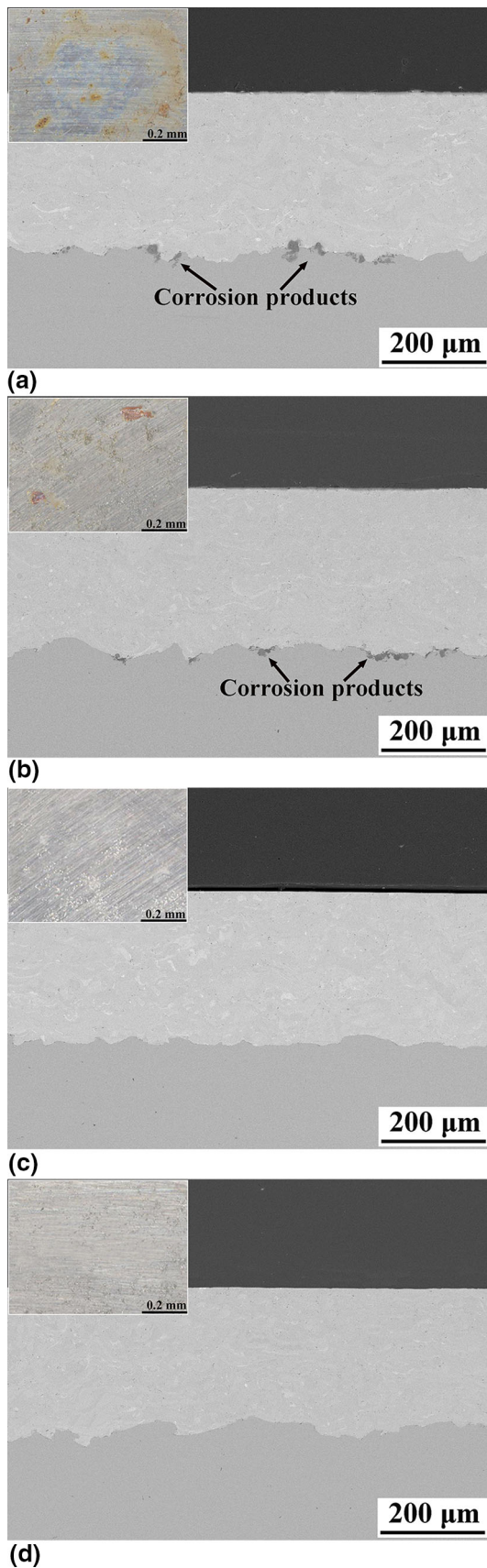
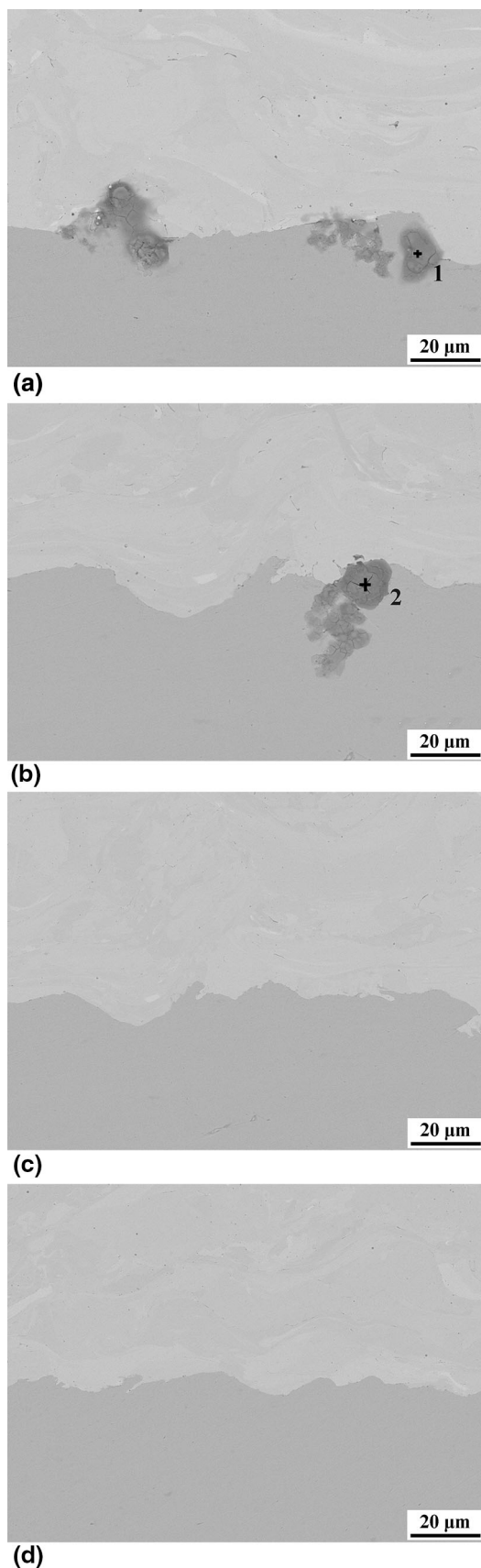


Fig. 9 Cross-sectional microstructure and surface morphologies (the insets) of different coatings after corrosion: **a** as-plasma-sprayed NiCr-20Mo coating; **b** the one-pass shot-peened NiCr-20Mo coating; **c** the two-pass shot-peened NiCr-20Mo coating; **d** the three-pass shot-peened NiCr-20Mo coating

20Mo coating film, there is still a small fraction of through-thickness pores in the coating. Thus, the corrosion resistance of the plasma-sprayed NiCr-20Mo-coated Q235 steel sample was still a little inferior to that of the free-standing NiCr-20Mo coating film, although the electrochemical data shown in Table 2 are very close. The existence of through-thickness pores will lead to the corrosion of the substrate at the interface and consequently the spalling of the coating. Therefore, although the plasma-sprayed NiCr-20Mo coating has excellent corrosion resistance, it could not provide effective protection for substrate from corrosion since there exists little amount of through-thickness pores within coating.

When the post-spray shot peening treatment was applied to the plasma-sprayed NiCr-20Mo coating by one pass, the E_{ocp} and E_{corr} of the sample increased nobly further and the i_{corr} was decreased compared with that of the as-plasma-sprayed NiCr-20Mo-coated sample. Therefore, corrosion resistance of the one-pass shot-peened NiCr-20Mo-coated Q235 steel sample was improved compared with that of the sample without shot peening treatment. Nevertheless, it was still slightly inferior to that of the free-standing NiCr-20Mo coating film. The E_{ocp} data evidently suggest that through-thickness pores were still not completely sealed by densifying effect of shot peening. On the contrast, in the cases of the two-pass and three-pass shot-peened NiCr-20Mo-coated samples, their E_{ocp} , E_{corr} and i_{corr} became comparable with that the free-standing NiCr-20Mo coating film, which indicated that corrosion resistance of the two-pass and three-pass shot-peened NiCr-20Mo-coated samples was comparable with that of the free-standing NiCr-20Mo coating film despite the influence of the active substrate.

Furthermore, the cross-sectional microstructure of the tested samples after corrosion test was examined, as shown in Fig. 9 and 10. Moreover, the corrosion morphologies of the tested samples surface are illustrated as insets in Fig. 9. On one hand, it was evidently observed from Fig. 9(a) and (b), 10(a) and (b) that some corrosion products were formed at the coating–substrate interfaces for the as-plasma-sprayed NiCr-20Mo-coated Q235 steel sample and the one-pass shot-peened plasma-sprayed NiCr-20Mo-coated sample, which corresponds to the iron rusts found on the corroded surface of these two coated samples after corrosion test, as illustrated in insets in Fig. 9(a) and (b). EDS analyses were employed for the corrosion products at point 1 and point 2 in Fig. 10(a) and (b), and results are



◀**Fig. 10** Closer views at the coating–substrate interface of different coatings after corrosion: **a** as-plasma-sprayed NiCr-20Mo coating; **b** the one-pass shot-peened NiCr-20Mo coating; **c** the two-pass shot-peened NiCr-20Mo coating; **d** the three-pass shot-peened NiCr-20Mo coating

Table 3 Chemical composition of the corrosion products at interface

Elemental composition (wt.%)	Point 1	Point 2
O	31.9	28.3
Fe	62.3	64.1
Cl	5.8	7.6

listed in Table 3. It was found that the corrosion products were oxide of iron and chloride, which revealed that the corrosion of the substrates in two samples occurred by the solution permeated through the small amount of tiny through-thickness pores within coating. In the case of the one-pass shot-peened NiCr-20Mo-coated Q235 steel, although a dense top layer with a thickness of about 100 μm was formed, the top dense layer of certain roughness may be possibly ground off during the preparation of the test sample to have a polished uniform surface. Then, the under-layer with tiny pores was exposed to corrosive medium. Consequently, the corrosion of substrate occurred by the permeated solution.

On the other hand, in the case of the shot-peened NiCr-20Mo-coated Q235 steel samples, when the shot peening passes reached or exceeded two times, as can be seen in Fig. 9(c) and (d), 10(c) and (d), the coating–substrate interfaces were clean with no corrosion products, which were the same as that observed in the coatings before corrosion tests. Moreover, no iron rust was clearly observed on the corroded surface of these two coated sample after test. This indicates that no substrate corrosion occurred for these samples. In this way, the coatings were protective due to complete barrier effect of the thick dense top layer. Therefore, it can be concluded that when the dense top layer was equivalent or thicker than 200 μm by a two or more than two-pass post-spray shot peening treatment, an effective barrier can be formed to prevent the penetration of the corrosive medium and finally protect the substrate from corrosion totally and effectively.

It is worth mentioning that besides the densification effect induced by shot peening, which has been proved above to contribute to improving the corrosion resistance of the coating, it has also been demonstrated that the residual stress in the subsurface region of the coating will change toward negative by the successive impact of the shot peening particles (Ref 34, 40), which will improve the stress corrosion resistance of the coating (Ref 41, 42).

Meanwhile, it has been revealed that more active sites for corrosion that would be formed after shot peening, resulting from the dislocation multiplication and grain nanosizing attributing to the severe plastic deformation of particles induced by peening (Ref 36, 38, 43), may, however, decrease the corrosion resistance of the coating (Ref 44, 45). Nevertheless, our recent experimental results have revealed that the post-spray shot peening has basically no influence on the corrosion resistance of the free-standing NiCr-20Mo coating film without substrate. Moreover, the different passes shot-peened free-standing NiCr-20Mo coating film presents comparable E_{ocp} , E_{corr} and i_{corr} to that of the as-plasma-sprayed free-standing NiCr-20Mo coating film. That is, the comprehensive effect of the residual stress and activation on corrosion is negligible compared to the densification effect induced by shot peening. Accordingly, the densification effect on corrosion is dominant and the change in the corrosion resistance induced by the residual stress and activation can be ignored. As a result, as the electrochemical test results are shown in Fig. 8 and 9, the two- and three-pass shot-peened NiCr-20Mo coating can provide the substrate with excellent and completely corrosion protection.

Conclusions

NiCr-20Mo coating was prepared by plasma spraying of the Mo-clad-NiCr powders to obtain a dense coating with excellent interface bonding. Moreover, the post-spray shot peening treatment was conducted for the plasma-sprayed NiCr-20Mo coating to obtain a fully dense coating through thoroughly closing off a little amount of through-thickness pores and un-bonded interfaces within coating. Corrosion behaviors of the NiCr-20Mo coatings before and after post-spray shot peening were tested to investigate the effect of post-spray shot peening on the corrosion behaviors of the NiCr-20Mo coating. Results showed that a dense and uniform coating with near-perfect bonding at most of interfaces was obtained for the as-plasma-sprayed NiCr-20Mo coating due to the impact-induced substrate surface melting through the novel shell-core powder design, although very little amount of tiny pores and un-bonded interfaces were present within coating. Furthermore, when the NiCr-20Mo coating was subjected to the post-spray shot peening applied by cold spraying of steel shots, the pores and un-bonded interfaces in the coating were fully closed off and a dense coating layer was formed by the tamping effect of the shot peening particles. In addition, with the increase in the shot peening intensity from one pass to three passes, the dense top layer became thicker from 100 to 200 μm , and finally to 300 μm of the whole coating thickness, which indicated a fully dense bulk-like

coating. Corrosion test results showed that corrosion resistance of the as-plasma-sprayed NiCr-20Mo coating improved significantly compared with that of the NiCr-coated Q235 steel due to the excellent bonding at most of lamellar interfaces within coating, although it was still a little inferior to that of the free-standing NiCr-20Mo coating film. Moreover, for the shot-peened NiCr-20Mo coatings, an effective barrier can be formed to prevent the penetration of the corrosive medium and make full protection of the substrate from corrosion effectively.

Therefore, a fully dense bulk-like NiCr-20Mo coating with excellent corrosion resistance can be achieved through the plasma spraying of Mo-clad-NiCr powders followed by appropriate post-spray shot peening treatment.

Acknowledgments The present project is financially supported by National Nature Science Foundation of China (Approved No.: 51474171).

References

1. A.H. Heuer, H. Kahn, F. Ernst, G.M. Michal, D.B. Hovis, R.J. Rayne, F.J. Martin, and P.M. Natishan, Enhanced Corrosion Resistance of Interstitially Hardened Stainless Steel: Implications of a Critical Passive Layer Thickness for Breakdown, *Acta Mater.*, 2012, **60**(2), p 716-725
2. J.E. Gray and B. Luan, Protective Coatings on Magnesium and Its Alloys—A Critical Review, *J. Alloys Comp.*, 2002, **33**(26), p 88-113
3. C.K. Tan and D.J. Blackwood, Corrosion Protection by Multi-layered Conducting Polymer Coatings, *Corros. Sci.*, 2003, **45**(3), p 545-557
4. M.K. Totlani and S.N. Athavale, Electroless Nickel for Corrosion Control in Chemical, Oil and Gas Industries: Corrosion Reviews, *Corros. Rev.*, 2000, **18**(2–3), p 155-180
5. A.L. Rudd, C.B. Breslin, and F. Mansfeld, The Corrosion Protection Afforded by Rare Earth Conversion Coatings Applied to Magnesium, *Corros. Sci.*, 2000, **42**(2), p 275-288
6. A.Y. Simaranov, A.I. Marshakov, and YuN Mikhailovskii, Formation of Conversion Coatings on Magnesium in Moderately Acid Chromate Solutions, *Prot. Met.*, 1990, **25**(5), p 611-618
7. C.K. Mittal, Chemical Conversion, and Anodized Coatings, *Trans. Met. Finish. Assoc. India*, 1995, **4**(4), p 227-237
8. B.R.W. Hinton, D.R. Arnott, and N.E. Ryan, Cerium Conversion Coatings for the Corrosion Protection of Aluminum, *Mater. Forum*, 1986, **9**(3), p 162-173
9. R. Feurer, N. Bui, R. Morancho, M. Larhafi, and R. Calsou, Electrochemical Behaviour of Molybdenum Based Coatings Obtained by Organometallic Chemical Vapour Deposition, *Br. Corros.*, 1989, **24**(2), p 126-130
10. J. Senf and E. Broszeit, Wear and Corrosion Protection of Aluminum and Magnesium Alloys Using Chromium and Chromium Nitride PVD Coatings, *Text. Res. J.*, 1999, **1**(2), p 133-137
11. C. Liu, Q. Bi, A. Leyland, and A. Matthews, An Electrochemical Impedance Spectroscopy Study of the Corrosion Behaviour of PVD Coated Steels in 0.5 N NaCl Aqueous Solution: Part I. Establishment of Equivalent Circuits for EIS Data Modelling, *Corros. Sci.*, 2003, **45**(6), p 1243-1256
12. Y.K. Wei, X.T. Luo, C.X. Li, and C.-J. Li, Optimization of In-Situ Shot-Peening-Assisted Cold Spraying Parameters for Full

- Corrosion Protection of Mg Alloy by Fully Dense Al-Based Alloy Coating, *J. Therm. Spray Technol.*, 2016, **26**(1–2), p 173–183
13. C.-J. Li, Y. Li, G.-J. Yang, and C.-X. Li, A Novel Plasma-Sprayed Durable Thermal Barrier Coating with a Well-Bonded YSZ Interlayer Between Porous YSZ and Bond Coat, *J. Therm. Spray Technol.*, 2012, **21**(3), p 383–390
 14. X.-T. Luo, Y.-K. Wei, Y. Wang, and C.-J. Li, Microstructure and Mechanical Property of Ti and Ti6Al4V Prepared by an In-Situ Shot Peening Assisted Cold Spraying, *Mater. Des.*, 2015, **85**, p 527–533
 15. G.P. Bierwagen, Corrosion Control by Organic Coatings, *Prog. Org. Coat.*, 1996, **28**(1), p 43–48
 16. H.F. Guo and A.N. Mao-Zhong, Electroplating and Electroless Plating on Magnesium and Magnesium Alloys, *Electroplat. Pollut. Control*, 2004, **24**(2), p 1–5
 17. J.B. Hajdu, E.F. Yarkosky, P.A. Cacciatore, and M.H. Suplicki, Electroless Nickel Process for Memory Disks, *Process. Devices*, 1990, **90**, p 685–690
 18. D. Crotty, C. Steinecker, and B. Durkin, Plating Difficult Substrates with Electroless Nickel, *Prod. Finish.*, 1996, **60**(4), p 44–49
 19. W.A. Fairweather, Electroless Nickel Plating of Magnesium, *Trans. Inst. Met. Finish.*, 1997, **75**(3), p 113–117
 20. Z. Zeng, S. Kuroda, and H. Era, Comparison of Oxidation Behavior of Ni-20Cr Alloy and Ni-Base Self-Fluxing Alloy During Air Plasma Spraying, *Surf. Coat. Tech.*, 2009, **204**(1–2), p 69–77
 21. A. Ohmori and C.-J. Li, Quantitative Characterization of the Structure of Plasma-Sprayed Al₂O₃ Coating by Using Copper Electroplating, *Thin Solid Films*, 1991, **201**(2), p 241–252
 22. C.-J. Li and A. Ohmori, Relationships Between the Microstructure and Properties of Thermally Sprayed Deposits, *J. Therm. Spray Technol.*, 2002, **11**(3), p 365–374
 23. C.-J. Li, G.-J. Yang, and C.-X. Li, Development of Particle Interface Bonding in Thermal Spray Coatings: A Review, *J. Therm. Spray Technol.*, 2012, **22**(2–3), p 192–206
 24. A. Ohmori, C.-J. Li, and Y. Arata, Influence of Plasma Spray Conditions on the Structure of Al₂O₃ Coatings (Surface Processing), *Trans. JWRI*, 1990, **19**(2), p 259–270
 25. C.-J. Li, A. Ohmori, and R. McPherson, The Relationship Between Microstructure and Young's Modulus of Thermally Sprayed Ceramic Coatings, *J. Mater. Sci.*, 1997, **32**(4), p 997–1004
 26. C.-J. Li, W.-Z. Wang, and Y. He, Measurement of Fracture Toughness of Plasma-Sprayed Al₂O₃ Coatings Using a Tapered Double Cantilever Beam Method, *J. Am. Ceram. Soc.*, 2003, **86**(8), p 1437–1439
 27. C.-J. Li, X.-J. Ning, and C.-X. Li, Effect of Densification Process on the Properties of Plasma-Sprayed YSZ Electrolyte Coatings for Solid Oxide Fuel Cell, *Surf. Coat. Tech.*, 2005, **190**(1), p 60–64
 28. B.D. Sartwell and R. McPherson, A Review of Microstructure and Properties of Plasma Sprayed Ceramic Coatings, *Surf. Coat. Tech.*, 1989, **39–40**(89), p 173–181
 29. R. McPherson, The Relationship Between the Mechanism of Formation, Microstructure and Properties of Plasma-Sprayed Coatings, *Thin Solid Films*, 1981, **83**(3), p 297–310
 30. V. Pershin, M. Lufitha, S. Chandra, and J. Mostaghimi, Effect of Substrate Temperature on Adhesion Strength of Plasma-Sprayed Nickel Coatings, *J. Therm. Spray Technol.*, 2002, **12**(3), p 370–376
 31. Y. Niu, X. Zheng, H. Ji, L. Qi, C. Ding, J. Chen, and G. Luo, Microstructure and Thermal Property of Tungsten Coatings Prepared by Vacuum Plasma Spraying Technology, *Fusion Eng. Des.*, 2010, **85**(7–9), p 1521–1526
 32. S. Deshpande, S. Sampath, and H. Zhang, Mechanisms of Oxidation and Its Role in Microstructural Evolution of Metallic Thermal Spray Coatings—Case Study for Ni-Al, *Surf. Coat. Tech.*, 2006, **200**(18–19), p 5395–5406
 33. J.-J. Tian, S.-W. Yao, X.-T. Luo, C.-X. Li, and C.-J. Li, An Effective Approach for Creating Metallurgical Self-Bonding in Plasma-Spraying of NiCr-Mo Coating by Designing Shell-Core-Structured Powders, *Acta Mater.*, 2016, **110**, p 19–30
 34. P. Zhang and J. Lindemann, Influence of Shot Peening on High Cycle Fatigue Properties of the High-Strength Wrought Magnesium Alloy AZ80, *Scr. Mater.*, 2005, **52**(6), p 485–490
 35. P. Zhang and J. Lindemann, Effect of Roller Burnishing on the High Cycle Fatigue Performance of the High-Strength Wrought Magnesium Alloy AZ80, *Scr. Mater.*, 2005, **52**(10), p 1011–1015
 36. P.C. King, S.H. Zahiri, and M. Jahedi, Microstructural Refinement Within a Cold-Sprayed Copper Particle, *Metall. Mater. Trans. A*, 2009, **40**(9), p 2115–2123
 37. Q. Wang, N. Birbilis, and M.X. Zhang, Interfacial Structure Between Particles in an Aluminum Deposit Produced by Cold Spray, *Mater. Lett.*, 2011, **65**(11), p 1576–1578
 38. H. Koivuluoto and P. Vuoristo, Structure and Corrosion Properties of Cold Sprayed Coatings: A Review, *Surf. Eng.*, 2014, **30**(6), p 404–413
 39. ASTM Designation C633, *Am. Soc. Test. Mater.*, 1982, **2**, p 636–642
 40. R. Ghelichi, D. Macdonald, S. Bagherifard, H. Jahed, M. Guagliano, and B. Jodoin, Microstructure and Fatigue Behavior of Cold Spray Coated Al5052, *Acta Mater.*, 2012, **60**(19), p 6555–6561
 41. Y. Wang, K.Y. Li, F. Scenini, J. Jiao, S.J. Qu, Q. Luo, and J. Shen, The Effect of Residual Stress on the Electrochemical Corrosion Behavior of Fe-based Amorphous Coatings in Chloride-Containing Solutions, *Surf. Coat. Tech.*, 2016, **302**(27–38), p 27–38
 42. S.H. Wang, S.H. Shan, and Y.C. Pan, Residual Stress and its Effect on Corrosion Behaviour of Butt Jointed Cu-Al Alloys, *Sci. Technol. Weld. Join.*, 1999, **4**(3), p 182–186
 43. X.T. Luo, C.X. Li, F.L. Shang, G.J. Yang, Y.Y. Wang, and C.J. Li, High Velocity Impact Induced Microstructure Evolution During Deposition of Cold Spray Coatings: A review, *Surf. Coat. Tech.*, 2014, **254**(10), p 11–20
 44. K.S. Raja, S.A. Namjoshi, and M. Misra, Improved Corrosion Resistance of Ni-22Cr-13Mo-4W Alloy by Surface Nanocrystallization, *Mater. Lett.*, 2005, **59**(5), p 570–574
 45. K. Balani, T. Laha, A. Agarwal, J. Karthikeyan, and N. Munroe, Effect of Carrier Gases on Microstructural and Electrochemical Behavior of Cold-Sprayed 1100 Aluminum Coating, *Surf. Coat. Tech.*, 2005, **195**(2–3), p 272–279